Urea-Dependent Unfolding of Murine Adenosine Deaminase: Sequential Destabilization As Measured by ^{19}F NMR†

Qin Shu and Carl Frieden*

Department of Biochemistry and Molecular Biophysics, Washington University School of Medicine, St. Louis, Missouri 63110

Received September 12, 2003; Revised Manuscript Received December 9, 2003

ABSTRACT: Murine adenosine deaminase (mADA) is a 40 kDa $(\beta/\alpha)_8$-barrel protein consisting of eight central β-strands and eight peripheral α-helices containing four tryptophan residues. In this study, we investigated the urea-dependent behavior of the protein labeled with 6-fluorotryptophan (6-^{19}F-Trp). The ^{19}F NMR spectrum of 6-^{19}F-Trp-labeled mADA reveals four distinct resonances in the native state and three partly overlapped resonances in the unfolded state. The resonances were assigned unambiguously by site-directed mutagenesis. Equilibrium unfolding of 6-^{19}F-Trp-labeled mADA was monitored using ^{19}F NMR based on these assignments. The changes in intensity of folded and unfolded resonances as a function of urea concentration show transition midpoints consistent with data observed by far-UV CD and fluorescence spectroscopy, indicating that conformational changes in mADA during urea unfolding can be followed by ^{19}F NMR. Chemical shifts of the ^{19}F resonances exhibited different changes between 1.0 and 6.0 M urea, indicating that local structures around 6-^{19}F-Trp residues change differently. The urea-induced changes in local structure around four 6-^{19}F-Trp residues of mADA were analyzed on the basis of the tertiary structure and chemical shifts of folded resonances. The results reveal that different local regions in mADA have different urea-dependent behavior, and that local regions of mADA change sequentially from native to intermediate topologies on the unfolding pathway.

Adenosine deaminase (ADA,[1] EC 3.5.4.4), catalyzing the irreversible deamination of adenosine (2′-deoxyadenosine) to inosine (2′-deoxyinosine) and ammonia, is a zinc metalloenzyme that is critical in purine metabolism and development of the immune system. Inherited ADA deficiency is associated with an autosomal recessive immunodeficiency disorder of varying severity. Approximately 20% of individuals with severe combined immunodeficiency (SCID) syndrome are deficient in ADA activity (*1*, *2*). The X-ray crystal structure of murine ADA (352 amino acid residues, 40 kDa) is a $(\beta/\alpha)_8$- or triosephosphate isomerase (TIM)-barrel (*3*), each molecule consisting of eight central β-strands and eight peripheral α-helices with a deep pocket in which the catalytic zinc and the substrate analogue are bound and sequestered (Figure 1). The protein sequence of murine ADA is 83% identical and more than 90% homologous to that of human ADA.

The $(\beta/\alpha)_8$- or TIM-barrel is one of the most common protein folds, comprising more than 10% of enzymes with known structure, and is an extreme example of the "one fold−many functions" paradigm (*4*−*6*). Folding studies on different $(\beta/\alpha)_8$-barrel proteins suggest complex mechanisms, although the proteins appear to have a similar domain structure. A "6+2" folding model is commonly accepted, mainly based on the fragment complementation studies of *N*-(5′-phosphoribosyl)anthranilate isomerase from *Saccharomyces cerevisiae* (*7*) and the α-subunit of tryptophan synthase (*8*, *9*). In this model, the first six β/α-units of $(\beta/\alpha)_{1-6}$ prefold in a native-like form to serve as a template for the association and folding of the unstructured last two β/α-units, $(\beta/\alpha)_{7-8}$. On the other hand, the $(\beta/\alpha)_8$-barrel imidazole glycerol phosphate synthase (HisF) was cleaved into two folded halves and assembled to form the stoichiometric and catalytically active HisF−NC complex by coexpression *in vivo* or joint refolding *in vitro*, supporting a "4+4" folding mechanism for HisF (*10*). Recent folding studies on the prototypical $(\beta/\alpha)_8$-barrel triosephosphate isomerase by misincorporation proton-alkyl exchange (MPAX) suggest a "3+3+2" model with three cooperatively unfolding subdomains with the same C-terminal domain, $(\beta/\alpha)_{7-8}$, but two N-terminal domains (*11*). The conservation of the folding mechanism in TIM-barrels is still ambiguous.

In this work, we have used ^{19}F NMR combined with 6-^{19}F-Trp labeling to study the folding mechanism of $(\beta/\alpha)_8$-barrel mADA. ^{19}F NMR spectroscopy is a powerful technique for following the equilibrium or kinetic process of protein folding and for revealing site-specific local structural changes. A folding intermediate in equilibrium with the native and unfolded forms of intestinal fatty acid binding protein (IFABP) was identified involving the region of Trp82 using

† This work is supported by NIH Grant DK13332 to C.F.

* To whom correspondence should be addressed: Department of Biochemistry and Molecular Biophysics, Washington University School of Medicine, 660 S. Euclid Ave., St. Louis, MO 63110. Telephone: (314) 362-3344. Fax: (314) 362-7183. E-mail: frieden@biochem.wustl.edu.

[1] Abbreviations: ADA, adenosine deaminase; mADA, murine adenosine deaminase; WT, wild type; W-F, tryptophan to phenylalanine; DHFR, dihydrofolate reductase; DTT, dithiothreitol; IPTG, isopropyl β-D-thiogalactopyranoside; 6-^{19}F-Trp, 6-fluorotryptophan; EDTA, ethylenediaminetetraacetic acid; CD, circular dichroism.

10.1021/bi035651x CCC: $27.50
Published on Web 01/21/2004

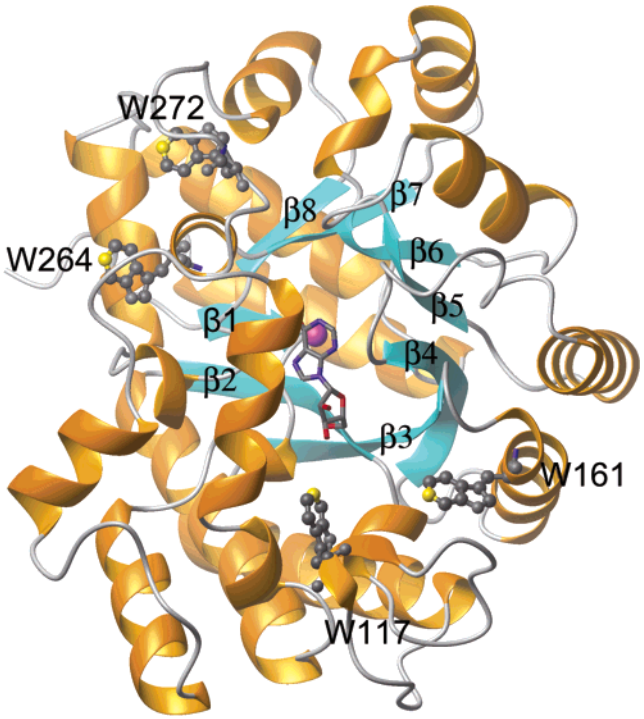

FIGURE 1: MOLMOL (*38*) representation of murine adenosine deaminase based on the 2.4 Å resolution X-ray crystal structure determined by Wilson et al. (*3*). The central β-barrel (viewed from the top of the active pocket) is shown in blue, and each of the eight β-strands is labeled. The α-helices are shown in orange. The metal cofactor, zinc (shown in purple), and the substrate analogue are located in the central active pocket. The four tryptophan residues are shown in ball-and-stick representations. The fluorinated C-6 atom on each indole ring of tryptophan is shown in yellow. W117 is located in the connecting loop between β2 and α2, W161 in α3, and W264 and W272 are located in the connecting loop between β7 and α7.

^{19}F NMR and protein labeled with 6-^{19}F-Trp (*12*). In the folding study of 5-^{19}F-Trp-labeled *Escherichia coli* D-lactate dehydrogenase by ^{19}F NMR, partially folded intermediates were observed, and different regions of the protein were shown to unfold nonuniformly as measured by the chemical shift changes, nuclear Overhauser effects, and solvent-induced isotopic shift effects (*13*). Real-time and equilibrium ^{19}F NMR studies of 6-^{19}F-Trp-labeled chaperone PapD revealed an intermediate in the C-terminal domain and provided insight into the role of domain−domain interaction in the folding of the protein containing two structural domains (*14*). The folding reaction of *E. coli* dihydrofolate reductase (DHFR) reveals several kinetic phases whose structural nature is obscure. Hoeltzli and Frieden followed the structural changes related to side chain environments of the five tryptophan residues of 6-^{19}F-Trp-labeled *E. coli* DHFR during denaturant-induced unfolding and refolding by using stopped-flow ^{19}F NMR spectroscopy (*15*−*18*). They showed that stabilization of the tryptophan side chains was the last step in the folding process (*19*). The high chemical shift resolution (100-fold larger than that of ^{1}H), coupled with the high sensitivity of ^{19}F nuclear spin, no background signals, easy incorporation at specific labeling sites, and minimal perturbation of the protein structure, yields well-resolved ^{19}F resonances in one-dimensional spectra (*20*, *21*). A ^{19}F NMR cryoprobe allows lower protein concentrations and shorter spectral acquisition times (*14*). All these facilitate the application of this technique in investigating the folding process of proteins, especially larger proteins whose folding mechanisms are more complicated than those of smaller proteins.

Murine adenosine deaminase contains four tryptophan residues that are conserved in the known mammalian enzyme, and are located in elements of the $(\beta/\alpha)_8$-barrel distant from the central β-barrel and the active site (Figure 1). These residues can serve as probes for detecting structural changes of different regions of the protein by ^{19}F NMR after incorporation of 6-^{19}F-Trp into the protein. The ^{19}F resonances of 6-^{19}F-Trp of mADA are well resolved in one-dimensional spectra. We have unambiguously assigned all of resonances in both the native and unfolded state by site-directed mutagenesis. Equilibrium unfolding of 6-^{19}F-Trp-labeled mADA was monitored using ^{19}F NMR on the basis of the assignments. The results reveal that mADA unfolds nonuniformly with different local regions around different tryptophan residues showing different urea-dependent conformation change behavior. The peripheral helices of the $(\beta/\alpha)_8$-barrel protein mADA, where W161 is located, are most susceptible to denaturant. The ^{19}F NMR data also show that different local regions of mADA sequentially change from native to specific and heterogeneous native-like or intermediate topologies as a function of the urea concentration on the unfolding pathway. The results provide a basis for investigating the folding kinetics of mADA and folding mechanisms of $(\beta/\alpha)_8$-barrel proteins by using ^{19}F NMR. The results are consistent with the observation that multiple intermediates and/or folding units exist in the folding of other $(\beta/\alpha)_8$-barrel proteins detected by different techniques.

MATERIALS AND METHODS

Materials. Ultrapure urea was a product of United States Biomedical. The concentration of urea was determined by the refractive index at 25 °C (*22*). 6-Fluoro-DL-tryptophan (6-^{19}F-Trp) was from Sigma. Restriction endonucleases were from New England Biolabs. Oligodeoxynucleotide primers used in constructions and mutations were synthesized at Sigma Genosys. *E. coli* strains XL1-Blue and XL2-Blue (Stratagene) were used for plasmid propagation, and strain W3110trpA33 which is auxotrophic for tryptophan (*12*, *14*, *15*, *23*) was used for the expression of unlabeled or 6-^{19}F-Trp-labeled mADA. All other chemicals were analytical-grade. The pQE sequencing primer set (QIAGEN) was used for the DNA sequencing of constructs.

Constructs. The expression plasmids of wild-type (WT) mADA and tryptophan to phenylalanine (W-F) mutants were derived from the pQE80-L vector (QIAGEN), which contained an isopropyl β-D-thiogalactopyranoside-inducible T5 promoter and provided sufficiently strict expression control. The mADA cDNA was amplified by PCR from the template plasmid prepared from AR120 pots/ADA NE5 (*24*). The forward primer is 5′-CCCGAATTCATTAAAGAGGAGAAATTAACTATGGCCCAGACACCCGC-3′ with an *Eco*RI site, an RBS sequence, and the start codon. The reverse primer is 5′-CCGAGCTCTTACTATTGGTATTCTCTGTAGAGCC-3′ with a *Sac*I site. The PCR products were purified with the QIAGEN PCR kit and used as inserts. This mADA cDNA was inserted into the pQE-80L vector through the *Eco*RI and *Sac*I sites and named pQE-80LmADA.

Tryptophan to phenylalanine mutations were introduced into the wild-type mADA cDNA in the construct of pQE-80LmADA with the QuikChange site-directed mutagenesis kit (Stratagene) using the following primers: W117F, 5′-GGTGGACCCAATGCCCTTCAACCAGACTGAAGGG-3′ (forward) and 5′-CCCTTCAGTCTGGTTGAAGGGCATT-GGGTCCACC-3′ (reverse); W161F, 5′-GCGCCACCAGC-CCAGCTTCTCCCTTGAGGTGTTGG-3′ (forward) and 5′-CCAACACCTCAAGGGAGAAGCTGGGCTGGTGGCGC-3′ (reverse); W264F, 5′-GCACTTTGAGGTCTGCCCC-TTCTCCAGCTACCTCACAGG-3′ (forward) and 5′-CCT-GTGAGGTAGCTGGAGAAGGGGCAGACCTCAAAGT-GC-3′ (reverse); and W272F, 5′-GCTACCTCACAGGCGC-CTTCGATCCCAAAACGACG-3′ (forward) and 5′-CGT-CGTTTTGGGATCGAAGGCGCCTGTGAGGTAGC-3′ (reverse). All constructs were sequenced to ensure their integrity and accuracy.

Expression and Purification of mADA. The wild-type or mutant constructs of pQE-80LmADA were transformed into *E. coli* strain W3110trpA33. For the expression of the unlabeled protein, bacteria were grown in Luria-Bertani (LB) medium at 37 °C and induced at an OD_{600} of ∼1.0 with 0.5 mM isopropyl β-D-thiogalactopyranoside (IPTG). Cells were grown for an additional 5 h and harvested by centrifugation. For the expression of 6-^{19}F-Trp-labeled WT mADA or W-F mutants (except for W161F), cells were grown in LB medium to an OD_{600} of ∼2.0 and harvested by centrifugation. To increase the labeling yield, cell pellets were washed using 6-^{19}F-Trp labeling medium without tryptophan and centrifuged two times. The washed cell pellets were resuspended and switched into 6-^{19}F-Trp labeling medium in the same volume of the original LB culture. After growing for 30 min, the culture was induced with 0.5 mM IPTG for 3−4 h and harvested. The 6-^{19}F-Trp labeling medium is similar to the labeling medium used elsewhere (*25*, *26*).

Under the same conditions for expression, W161F appeared in inclusion bodies. To express this protein, bacteria were grown at 25 °C and induced for 2 h. This procedure resulted in protein in both the soluble fraction and inclusion bodies. It was purified from the soluble fraction.

WT mADA and the W-F mutants were purified essentially as previously described (*27*−*29*). The supernatant of the crude cell lysate was purified using a HiTrap Q HP column (Amersham Biosciences) with the ÄKTA FPLC system. The mADA-containing fractions were pooled and brought to 50% saturation with solid ammonium sulfate. After centrifugation, the supernatant was brought to 80% saturation and centrifuged. The pellets were dissolved in a buffer of 20 mM potassium phosphate (pH 7.4), 2 mM DTT, and 1.7 N $(NH_4)_2SO_4$ and purified by using a hydrophobic interaction chromatography column packed with Butyl Sepharose 4 Fast Flow medium (Amersham Pharmacia Biotech). The pooled fractions containing mADA were concentrated by ultrafiltration using YM10 membranes (Amicon) and purified by gel filtration on a HiPrep 16/60 Sephacryl S-200 column. The purity of mADA was assessed by SDS−PAGE. The 6-^{19}F-Trp labeling yield was shown to be greater than 90% as measured by ESI mass spectroscopy. Protein concentrations were determined using the Bio-Rad protein assay reagent.

Enzyme Assays and Kinetic Analyses. Enzymatic activity was assayed on a Cary50Bio spectrophotometer (Varian) by measuring the rate of the ADA-dependent decrease in adenosine absorption at 265 nm and 20 °C, using a difference extinction coefficient of 8.5 mM^{-1} cm^{-1} (*27*−*29*). One unit of ADA activity is defined as the amount of enzyme that produced 1 μmol of inosine per minute. Cuvettes with a path length of 1 cm were used. Assays were carried out in a buffer of 20 mM potassium phosphate (pH 7.4) and 0.1 mM EDTA, with 75 μM adenosine. The enzyme concentration in the assay mixture was 1 or 5 nM as determined by titration with deoxycoformycin.

Equilibrium Unfolding Monitored by CD and Fluorescence Spectrometry. The unlabeled and 6-^{19}F-Trp-labeled mADA were unfolded at urea concentrations from 0 to 9.0 M in 20 mM Tris-HCl (pH 7.4) and 2 mM DTT and equilibrated at room temperature for 22 h. The far-UV CD spectra were measured on a Jasco-J715 spectropolarimeter with a 0.1 cm path length cell using 10 μM protein at 20 °C. Spectra were recorded from 180 or 200 to 250 nm. The fluorescence emission spectrum was measured on a PTI fluorometer (Photon Technology International, Inc.) using 1 μM protein at 20 °C. Since 6-^{19}F-Trp-labeled and unlabeled mADA differ in quantum yield and emission maximum, the fluorescence emission was measured at 330 nm for unlabeled and 340 nm for 6-^{19}F-Trp-labeled mADA.

^{19}F NMR Experiments. NMR spectra were recorded on a Varian Unity-Plus 500 MHz spectrometer operating at 470 MHz for ^{19}F nuclear spin using a Varian Cryo-Q dedicated 5 mm probe. The cryoprobe was maintained at 20 K with the Varian Cryo-Q Open Cycle Cryogenic system. The temperature of the sample was maintained at 20 °C with the XRII851 Air-Jet Crystal Cooler heat exchanger (FTS Systems, Stone Ridge, NY). The T_1 relaxation times were determined by the inversion recovery method. Data were acquired for 0.501 s using the Varian VNMR s2pul pulse sequence and a spectral width of 6499.8 Hz. All spectra were collected for 1024 transients in a buffer of 20 mM Tris-HCl (pH 7.4), 2 mM DTT, and 5% D_2O, with 0.2 mM 4-^{19}F-Phe as the internal chemical shift reference. For equilibrium unfolding experiments, 6-^{19}F-Trp-labeled WT mADA (85 μM) was equilibrated in 0−8.0 M urea at room temperature for 22 h.

RESULTS AND DISCUSSION

Properties of Unlabeled and 6-^{19}F-Trp-Labeled mADA

The unlabeled and 6-^{19}F-Trp-labeled WT mADA exhibit similar behavior during purification by ion exchange, hydrophobic interaction, and gel filtration FPLC (data not shown). The specific activity was ∼ 150 s^{-1}, and $K_m = 30 \pm 10$ μM for unlabeled and 6-^{19}F-Trp-labeled wild-type mADA as well as W-F mutants. The secondary structures of unlabeled and 6-^{19}F-Trp-labeled mADA are the same as measured by CD spectra (Figure 2A). 6-^{19}F-Trp-labeled mADA has a higher quantum yield, and the fluorescence emission maximum is shifted to the red by 5 nm relative to that of the unlabeled protein (Figure 2B). The urea denaturation curves of unlabeled and labeled proteins monitored by far-UV CD or intrinsic fluorescence spectroscopy are similar (panels C and D of Figure 2 and Table 2). These data indicate that the incorporation of 6-^{19}F-Trp into mADA (>90%) has little effect on the activity and structure of the protein.

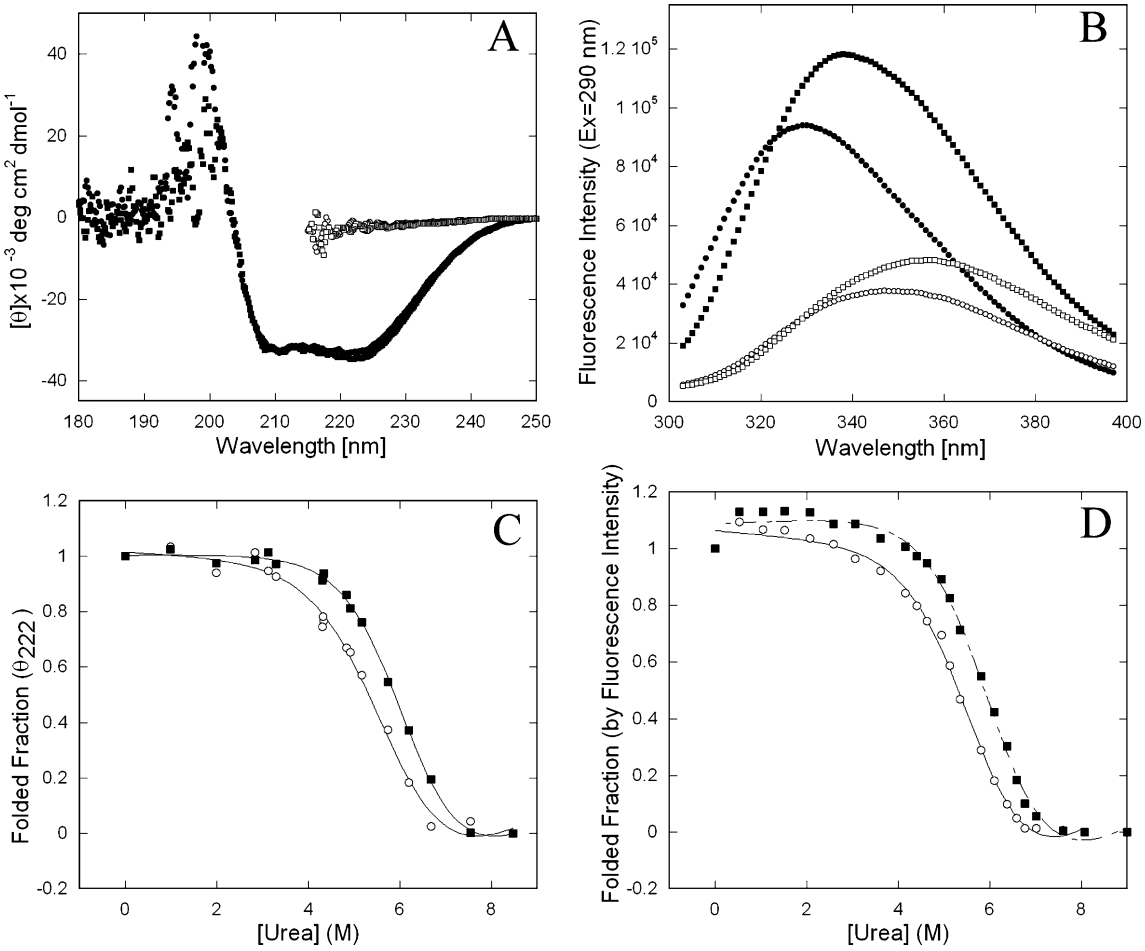

FIGURE 2: Effect of 6-^{19}F-Trp labeling on the structure and stability of mADA. (A) Far-UV CD and (B) fluorescence emission spectra of unlabeled (circles) and 6-^{19}F-Trp-labeled (squares) mADA in 0 M urea (filled symbols) or 8.0 M urea (empty symbols). (C) Unfolding curve of unlabeled (circles) and 6-^{19}F-Trp-labeled (squares) mADA monitored by CD and (D) by fluorescence spectroscopy. Ellipticities were measured at 222 nm, and fluorescence emissions were measured at 330 nm for unlabeled and at 340 nm for 6-^{19}F-Trp-labeled mADA. The solid lines show the fit to a two-state model (*22*). All experiments were carried out at 20 °C in 20 mM Tris-HCl (pH 7.4) and 2 mM DTT after equilibrium with urea had been established at room temperature for 22 h. The protein concentration is 1.0 μM for fluorescence and 10.0 μM for CD experiments.

Table 1: Parameters of ^{19}F for 6-^{19}F-Trp-Labeled WT mADA[a]

	native		unfolded (8 M urea, equilibrated for 22 h)	
residue	chemical shift (ppm)	line width (Hz)	chemical shift (ppm)	line width (Hz)
W117	−45.15	77.2	−46.15	44.1
W161	−48.19	65.3	−46.27[b]	48.1[b]
W264	−47.59	64.4	−46.27[b]	48.1[b]
W272	−47.03	65.3	−46.45	41.9

[a] Data were collected at 20 °C using 85 μM protein in 20 mM Tris-HCl (pH 7.4), 2 mM DTT, and 5% D_2O, with 0.2 mM 4-^{19}F-Phe as the internal chemical shift reference. The line widths were determined from spectra deconvoluted using a Bayesian analysis fitting routine (*30*). [b] The peaks of W161 and W264 overlap.

Assignment of ^{19}F NMR Resonances

The ^{19}F NMR spectra of 6-^{19}F-Trp-labeled WT mADA reveal four distinct resonances under native conditions and three partly overlapped resonances under unfolded conditions (Figure 3). To assign these resonances, four site-directed mutants of mADA (W117F, W161F, W264F, and W272F) were made, each with one tryptophan replaced by a phenylalanine. The mutants, all except W161F, were expressed and purified in a manner essentially similar to that of WT mADA. As shown in Figure 3, the ^{19}F NMR resonances of mADA can be unambiguously assigned (Table 1) by comparing the ^{19}F NMR spectra of WT mADA and mutants W117F, W264F, and W272F in native and unfolded states. The mutant W161F was not used because a second unknown peak was seen in the spectra (data not shown).

Equilibrium Unfolding of 6-^{19}F-Trp-Labeled mADA using ^{19}F NMR

Resonance Amplitudes as a Function of Urea Concentration. The equilibrium folding properties of 6-^{19}F-Trp WT mADA were investigated by ^{19}F NMR on the basis of the assignment results. The spectra collected at various urea concentrations (Figure 4) show that resonances in either the folded or unfolded state are well resolved in a one-dimensional spectrum. At different urea concentrations, the spectrum shows different mixtures of stable folded and unfolded resonances, which indicates a very slow rate of interconversion between folded and unfolded forms. With an increasing urea concentration, the intensities of unfolded resonances increase while those of folded resonances decrease. Deconvolution of all ^{19}F NMR spectra was performed using a Bayesian analysis program (*30*) to obtain the relative amplitudes of each resonance. Figure 5 shows the amplitude

Table 2: Equilibrium Unfolding Parameters of Unlabeled and 6-^{19}F-Trp-Labeled WT mADA by CD, Fluorescence, and ^{19}F NMR Spectroscopy[a]

experiment	sample	$\Delta G°$ (kcal/mol)	m (kcal mol^{-1} M^{-1})	$[\text{urea}]_{1/2}$ (M)
fluorescence intensity	unlabeled (Em = 330 nm)	5.17	0.85	6.08
	6-^{19}F-Trp-labeled (Em = 340 nm)	4.87	0.85	5.73
far-UV CD ellipticity at 222 nm	unlabeled	5.47	0.89	6.15
	6-^{19}F-Trp-labeled	4.44	0.77	5.77
^{19}F NMR amplitude of resonances	W117 folded (−45.15 ppm)[b]	7.40	1.31	5.65
	W161 folded (−48.19 ppm)[b]	13.14	2.48	5.30
	W264 folded (−47.59 ppm)[b]	13.08	2.28	5.74
	W272 folded (−47.03 ppm)[b]	5.69	1.05	5.42
	W117 unfolded (−46.15 ppm)[c]	10.96	1.96	5.59
	W161 and W264 unfolded (−46.27 ppm)[c]	10.42	1.87	5.57
	W272 unfolded (−46.45 ppm)[c]	12.55	2.25	5.58

[a] All spectroscopy experiments were performed at 20 °C in 20 mM Tris-HCl (pH 7.4) and 2 mM DTT. Equilibrium unfolding parameters were obtained from fitting the data to a two-state model (*22*). [b] As measured by the decrease in the amplitude of native resonances. [c] As measured by the increase in the amplitude of unfolded resonances.

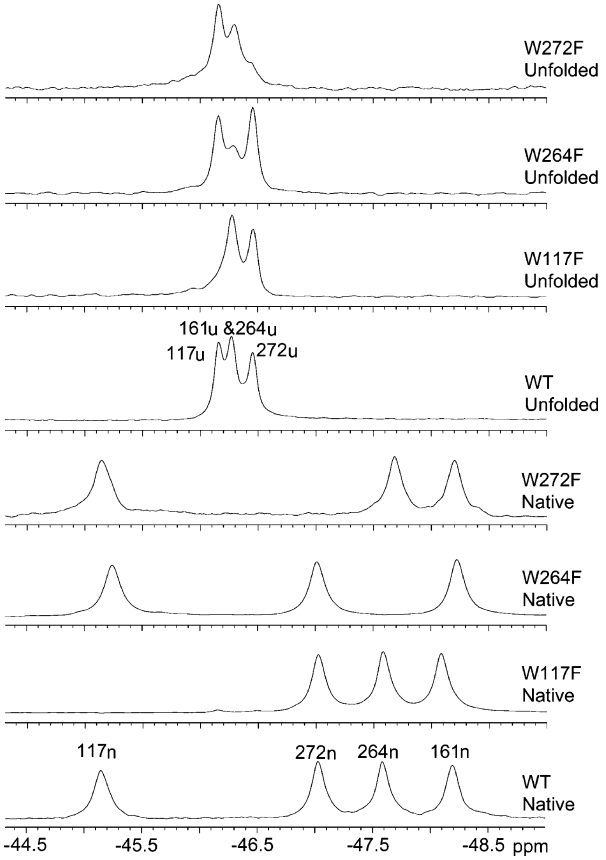

FIGURE 3: ^{19}F NMR spectra of WT 6-^{19}F-Trp-labeled mADA and W-F mutants (W117F, W264F, and W272F) in the native (0 M urea) or unfolded state (8.0 M urea, equilibrated at room temperature for 22 h). Spectra were recorded at 20 °C in 20 mM Tris-HCl (pH 7.4), 2 mM DTT, and 5% D_2O, with 0.2 mM 4-^{19}F−Phe as the internal chemical shift reference. The protein concentration was ~100 μM. The resonances of WT mADA in native (labeled with the residue number and the letter n) or unfolded states (labeled with the residue number and the letter u) were assigned by comparison of these spectra.

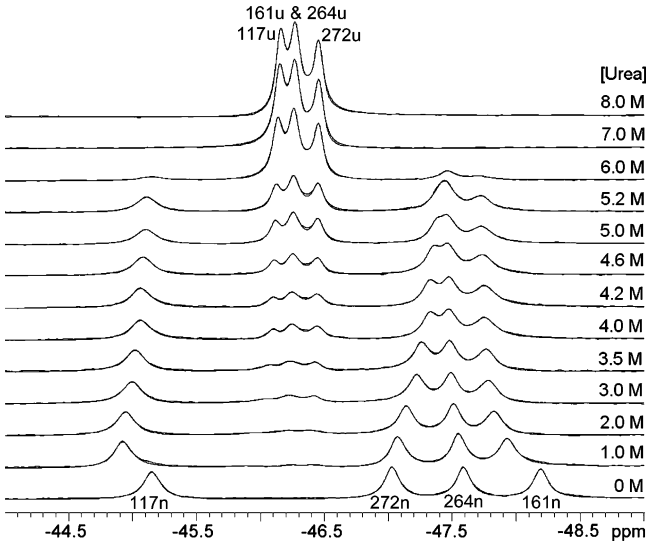

FIGURE 4: ^{19}F NMR spectra of 6-^{19}F-Trp-labeled mADA as a function of urea concentration. All spectra were collected at 20 °C using 85 μM protein in 20 mM Tris-HCl, 2 mM DTT (pH 7.4), and 5% D_2O, with 0.2 mM 4-^{19}F-Phe as an internal chemical shift reference. All samples were equilibrated at room temperature for 22 h before spectra were collected.

change in the folded (Figure 5A) and unfolded (Figure 5B) peaks as a function of urea concentration. The amplitude change was fitted with a two-state transition function for each peak. The fitting parameter of each resonance is similar to the denaturation midpoint obtained by CD and fluorescence spectroscopy (Table 2). The results confirm that the conformational change in mADA during urea unfolding can be followed by ^{19}F NMR using 6-^{19}F-Trp labeling.

The values of $\Delta G°$ and cooperativity index (m) derived from the fitting of ^{19}F NMR data, however, are greater than those from CD and fluorescence spectroscopy except for those of the W272 folded resonance (Table 2). One possibility is that at some unfolding stage different conformations of the protein molecule are in fast exchange so that some NMR signal cannot be detected. Partial loss of resonance intensity was also reported in the folding studies of other proteins using ^{19}F NMR (*12*, *17*). A more important possibility is due to the non-two-state behavior of the equilibrium unfolding of mADA revealed by ^{19}F NMR, which is shown more clearly by the chemical shift change of folded resonances.

Chemical Shifts as a Function of Urea Concentration. The spectra recorded between 1.0 and 6.0 M urea show that chemical shifts of folded resonances are affected differently by denaturants. The urea dependence of the chemical shift for each resonance relative to the native resonance is shown in Figure 6A. With an increasing urea concentration (from 1 to 6 M), the chemical shift of folded resonance W117 moves in a complex way (fitted with a double-exponential curve) that first shifts downfield 0.23 ppm relative to the

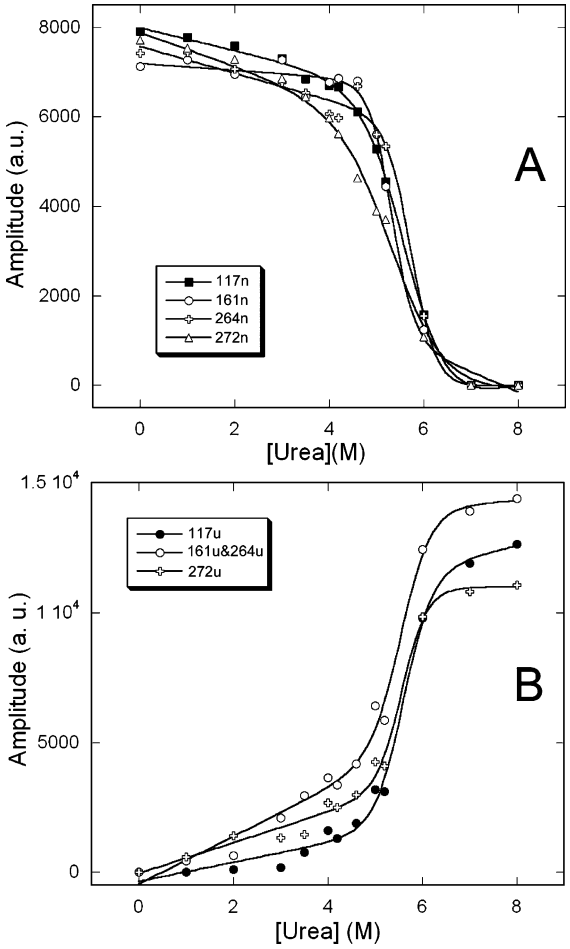

FIGURE 5: Change in the ^{19}F NMR resonance amplitude as a function of urea concentration (data from Figure 4). The amplitude was obtained by using Bayesian analysis: (A) folded resonances and (B) unfolded resonances. The fits to a two-state model (*22*) of folded and unfolded resonances are shown with solid lines.

native peak by 1 M urea and then shifts back to close to the native state. At 1 M urea, the resonance of W161 shifts downfield 0.26 ppm, which is similar to that for W117. Between 1 and 6 M urea, W161 exhibits the largest shift (downfield to 0.49 ppm) with a midpoint at ~0.75 M urea that is well below the unfolding midpoint of 5.7 M monitored by optical techniques. Above a urea concentration of 3.5 M, no further chemical shift occurs for W161, but the intensity of the peak decreases (Figures 4 and 6A). W272 shifts linearly upfield 0.04−0.43 ppm with a slope of ~0.08 and gradually merges with the peak of W264 at >3 M urea (Figure 4). W264 shifts linearly downfield 0.04−0.14 ppm with a slope of 0.02, which is possibly due to a solvent and/or urea effect since it is the most exposed Trp.

The chemical shift of the ^{19}F nucleus is extremely sensitive to changes in the local conformational environment, including van der Waals interactions and local electrostatic fields (*20*). In the cases of W117, W161, and W272, the large magnitude of the shift, the different shift direction, and complicated behavior suggest that the chemical shift changes are due to a local structure change rather than solvent effects. In the crystal structure, W117, W264, and W272 are more exposed to the solvent environment than W161. The solvent accessible surface areas calculated with the program GETAREA (*31*) for the side chain of each tryptophan and for the ^{19}F-substituted CH2 proton are 30.23 and 10.38 Å^2 for W117,

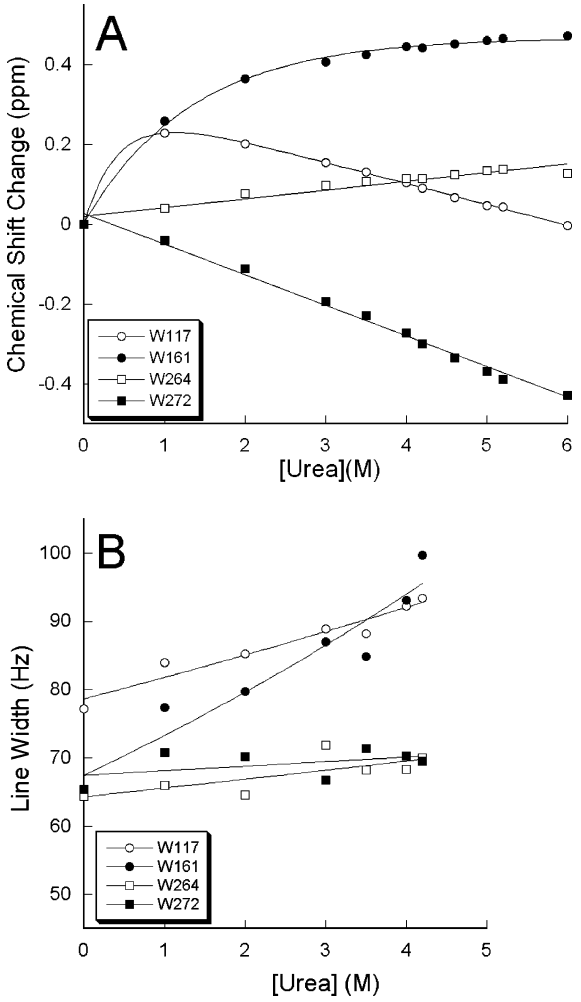

FIGURE 6: ^{19}F NMR chemical shift and line width change of each folded resonance as a function of urea concentration (data from Figure 4). (A) Chemical shift change. The chemical shift change of folded resonance W117 was fit to a double-exponential curve and W161 to a single-exponential function, and W264 and W272 were fit to linear curves. (B) Line width change. Data were derived from the Bayesian analysis. Solid lines are drawn to guide the eye.

13.46 and 4.48 Å^2 for W161, 62.73 and 24.25 Å^2 for W264, and 33.63 and 16.10 Å^2 for W272, respectively. W161 is the most buried residue in the structure, while W264 is the most exposed. The solvent/denaturant exposure level for the side chain and ^{19}F nucleus shows no correlation with the chemical shift change from the data of Figure 6A. We believe it would be more reasonable to suggest that the larger chemical shift change results from changes in the side chain environment and local structure for the more buried 6-^{19}F-Trp residues in mADA.

Figure 6B shows the line width of each folded resonance between 0 and 4.2 M urea representing the different relaxation of different resonances. Since all shifted resonances are single peaks, the resonance shift may result from fast or intermediate exchange of different conformations (the native and native-like or intermediate conformations). Noticeable peak broadening with an increasing urea concentration was observed for W117 and W161, indicating that the conformational exchange rates for W117 and W161 may slow with an increasing urea concentration. W264 and W272 have no obvious broadening with an increasing urea concentration.

In summary, the different chemical shift changes indicate that local structures around W117, W161, and W272 are not in their native conformation but in native-like or intermediate topologies, even though the protein is still native as implied by other biophysical techniques such as CD and fluorescence spectroscopy. The different urea-dependent chemical shift behavior for each 6-^{19}F-Trp resonance indicates that mADA behaves nonuniformly, and different local regions of mADA sequentially change from native to specific and heterogeneous native-like or intermediate topologies on the unfolding pathway.

Site-Specific Local Structure Change upon Urea-Induced Unfolding

The site-specific local structure change on urea-induced unfolding was analyzed on the basis of the tertiary structure of mADA and the chemical shift change of each folded resonance observed in ^{19}F NMR experiments. In the tertiary structure, all four tryptophan residues are located in different elements of secondary and tertiary structure (Figure 1). W117 is located in a small 3/10-helix of the large connecting loop between the central β2 strand and the peripheral α2 helix. W161 is located in the peripheral α3 helix. W264 and W272 are located in the large connecting loop between β7 and α7. W264 is in a short helix (residues 263−268), which is within this connecting loop. All of them are distant from the central β-barrel and the active site. Moreover, the four tryptophans in mADA can be divided into two groups by spatial distance; W117 and W161 are spatially adjacent, as are W264 and W272. The distance between two fluorine nuclei is ~8.5 Å for W117 and W161 and 9.2 Å for W264 and W272.

The small chemical shift change of the folded resonance of W264 as a function of urea concentration suggests that the local structure around W264 (probably the short helix in the connecting loop between β7 and α7) is basically conserved in the native conformation until the protein is completely denatured. Since W272 is near W264, the chemical shift behavior of resonance W272, upfield to merge with W264 at high urea concentrations (Figure 4), suggests that local structure around W272 probably changes to an intermediate topology that is closer to W264 at higher urea concentrations. The chemical shifts of W117 and W161 move downfield at 1.0 M urea and are more susceptible to a low urea concentration than those of W264 and W272 (Figure 6A). Since W117 and W161 are close to each other and distant from the other two tryptophans, the region around W117 and W161 is probably more sensitive to a low urea concentration-induced conformation change than the region around W264 and W272. As shown above, the line widths of W117 and W161 show similar broadening with an increasing urea concentration while W264 and W272 do not (Figure 6B). These results reflect the fact that ^{19}F NMR signal changes of these tryptophan residues in mADA correspond with their structural characteristics.

The chemical shift of W161 is almost independent of urea concentration above 3.5 M urea (Figures 4 and 6A), while the midpoint of the denaturation curve is ~5.7 M urea (Table 2). It indicates that local structure around W161 sequentially changes from the native to some stable intermediate conformation that is in slow exchange with the unfolded conformation and independent of urea concentration above 3.5 M. The chemical shift changes of all folded Trp resonances are completed above 4 M urea (Figures 4 and 6A), which suggests that mADA forms a relatively stable intermediate conformation that is independent of urea concentration above 4 M.

The chemical shift of W161 is the most sensitive to low urea concentrations and has the largest shift magnitude among four 6-^{19}F-Trp residues in mADA (Figures 4 and 6A). This suggests that the side chain environment and local structure of W161 are most sensitive to the denaturant during unfolding. Since W161 is the only tryptophan located in one of the eight peripheral α-helices of $(\beta/\alpha)_8$-barrel mADA, we hypothesize that the peripheral helices of mADA, where W161 is located, are most sensitive to denaturants during unfolding, which may cause side chain packing disruption and the peripheral hydrogen bond network to collapse. Further unfolding may result from loosening of the tightly organized peripheral helices, the loss of the hydrophobic interaction between parallel α-helices and β-strands, and the collapse of central β-sheets.

The challenge of protein folding studies for the experimentalist and theoretician is to cope with the small energetic changes and to devise methods for describing the behavior of the side chains and backbone at atomic resolution as the protein either folds or unfolds (*32*). The folding study of urea-induced equilibrium unfolding of mADA monitored by ^{19}F NMR combined with 6-^{19}F-Trp labeling provides information related to site-specific local structure change and side chain behavior as well as the properties of intermediates on the urea-induced unfolding pathway. The results are also consistent with the observation that multiple intermediates and/or folding units exist on the folding pathway as observed in other $(\beta/\alpha)_8$-barrel proteins detected by different techniques (*7*−*11*, *33*−*37*). Kinetic unfolding and refolding studies of mADA monitored by ^{19}F NMR are being carried out, which should help to interpret the current equilibrium unfolding data.

In conclusion, we have investigated the site-specific local structure change and properties of intermediates of mADA during urea-induced unfolding by ^{19}F NMR combined with 6-^{19}F-Trp labeling. The folding mechanism revealed by such a technique suggests that mADA unfolds nonuniformly and local regions of mADA sequentially change from native to specific and heterogeneous native-like or intermediate topologies on the unfolding pathway. This study also provides a basic for investigating folding kinetics of mADA and the conservation of the folding mechanism of $(\beta/\alpha)_8$-barrel proteins by the site-related ^{19}F NMR method.

ACKNOWLEDGMENT

We gratefully acknowledge Linda C. Kurz, James G. Bann, and Sydney D. Hoeltzli for helpful discussion, Robert Horton for technical assistance, and Vera Sideraki (Baylor College of Medicine, Houston, TX) for providing the AR120 pots/ADA NE5 strain.

REFERENCES

1. Giblett, E. R., Anderson, J. E., Cohen, F., Pollara, B., and Meuwissen, H. J. (1972) *Lancet 2*, 1067−1069.
2. Hershfield, M. S., and Mitchell, B. S. (1995) in *The Metabolic and Molecular Basis of Inherited Disease* (Scriver, C. R., Beaudet,

A. L., Sly, W. S., and Valle, D., Eds.) 7th ed., pp 1725−1768, McGraw-Hill, New York.
3. Wilson, D. K., Rudolph, F. B., and Quiocho, F. A. (1991) *Science 252*, 1278−1284.
4. Farber, G. K., and Petsko, G. A. (1990) *Trends Biochem. Sci. 15*, 228−234.
5. Nagano, N., Hutchinson, E. G., and Thornton, J. M. (1999) *Protein Sci. 8*, 2072−2084.
6. Nagano, N., Orengo, C. A., and Thornton, J. M. (2002) *J. Mol. Biol. 321*, 741−765.
7. Eder, J., and Kirschner, K. (1992) *Biochemistry 31*, 3617−3625.
8. Zitzewitz, J. A., Gualfetti, P. J., Perkons, I. A., Wasta, S. A., and Matthews, C. R. (1999) *Protein Sci. 8*, 1200−1209.
9. Zitzewitz, J. A., and Matthews, C. R. (1999) *Biochemistry 38*, 10205−10214.
10. Hocker, B., Beismann-Driemeyer, S., Hettwer, S., Lustig, A., and Sterner, R. (2001) *Nat. Struct. Biol. 8*, 32−36.
11. Silverman, J. A., and Harbury, P. B. (2002) *J. Mol. Biol. 324*, 1031−1040.
12. Ropson, I. J., and Frieden, C. (1992) *Proc. Natl. Acad. Sci. U.S.A. 89*, 7222−7226.
13. Sun, Z. Y., Pratt, E. A., Simplaceanu, V., and Ho, C. (1996) *Biochemistry 35*, 16502−16509.
14. Bann, J. G., Pinkner, J., Hultgren, S. J., and Frieden, C. (2002) *Proc. Natl. Acad. Sci. U.S.A. 99*, 709−714.
15. Hoeltzli, S. D., and Frieden, C. (1994) *Biochemistry 33*, 5502−5509.
16. Hoeltzli, S. D., and Frieden, C. (1995) *Proc. Natl. Acad. Sci. U.S.A. 92*, 9318−9322.
17. Hoeltzli, S. D., and Frieden, C. (1996) *Biochemistry 35*, 16843−16851.
18. Hoeltzli, S. D., and Frieden, C. (1998) *Biochemistry 37*, 387−398.
19. Frieden, C. (2003) *Biochemistry 42*, 12439−12446.
20. Danielson, M. A., and Falke, J. J. (1996) *Annu. Rev. Biophys. Biomol. Struct. 25*, 163−195.
21. Gerig, J. (1994) *Prog. Nucl. Magn. Reson. Spectrosc. 26*, 293−370.
22. Pace, C. N., and Scholtz, J. M. (1997) in *Protein structure: a practical approach* (Creighton, T. E., Ed.) pp 299−321, IRL Press at Oxford University Press, New York.
23. Drapeau, G. R., Brammar, W. J., and Yanofsky, C. (1968) *J. Mol. Biol. 35*, 357−367.
24. Cooper, B. F., Sideraki, V., Wilson, D. K., Dominguez, D. Y., Clark, S. W., Quiocho, F. A., and Rudolph, F. B. (1997) *Protein Sci. 6*, 1031−1037.
25. Muchmore, D. C., McIntosh, L. P., Russell, C. B., Anderson, D. E., and Dahlquist, F. W. (1989) *Methods Enzymol. 177*, 44−73.
26. Frieden, C., Hoeltzli, S. D., and Bann, J. G. (2003) *Methods Enzymol. 380* (in press).
27. Agarwal, R. P., and Parks, R. E., Jr. (1978) *Methods Enzymol. 51*, 502−507.
28. Nygaard, P. (1978) *Methods Enzymol. 51*, 508−512.
29. Sideraki, V., Mohamedali, K. A., Wilson, D. K., Chang, Z., Kellems, R. E., Quiocho, F. A., and Rudolph, F. B. (1996) *Biochemistry 35*, 7862−7872.
30. Bretthorst, G. L., Kotyk, J. J., and Ackerman, J. J. (1989) *Magn. Reson. Med. 9*, 282−287.
31. Fraczkiewicz, R., and Braun, W. (1998) *J. Comput. Chem. 19*, 319−333.
32. Fersht, A. R., and Daggett, V. (2002) *Cell 108*, 573−582.
33. Jasanoff, A., Davis, B., and Fersht, A. R. (1994) *Biochemistry 33*, 6350−6355.
34. Sanchez del Pino, M. M., and Fersht, A. R. (1997) *Biochemistry 36*, 5560−5565.
35. Bilsel, O., Zitzewitz, J. A., Bowers, K. E., and Matthews, C. R. (1999) *Biochemistry 38*, 1018−1029.
36. Morgan, C. J., Wilkins, D. K., Smith, L. J., Kawata, Y., and Dobson, C. M. (2000) *J. Mol. Biol. 300*, 11−16.
37. Forsyth, W. R., and Matthews, C. R. (2002) *J. Mol. Biol. 320*, 1119−1133.
38. Koradi, R., Billeter, M., and Wuthrich, K. (1996) *J. Mol. Graphics 14*, 51−55.

BI035651X